



**HAL**  
open science

## The summer 2012 Greenland heat wave: in situ and remote sensing observations of water vapor isotopic composition during an atmospheric river event

Jean-Louis Bonne, Hans Christian Steen-Larsen, Camille Risi, Martin Werner, Harald Sodemann, Jean-Lionel Lacour, Xavier Fettweis, Grégory Cesana, Marc Delmotte, Olivier Cattani, et al.

### ► To cite this version:

Jean-Louis Bonne, Hans Christian Steen-Larsen, Camille Risi, Martin Werner, Harald Sodemann, et al.. The summer 2012 Greenland heat wave: in situ and remote sensing observations of water vapor isotopic composition during an atmospheric river event. *Journal of Geophysical Research: Atmospheres*, 2015, 120 (7), pp.2970-2989. 10.1002/2014JD022602 . hal-01116711

**HAL Id: hal-01116711**

**<https://hal.science/hal-01116711>**

Submitted on 16 Aug 2020

**HAL** is a multi-disciplinary open access archive for the deposit and dissemination of scientific research documents, whether they are published or not. The documents may come from teaching and research institutions in France or abroad, or from public or private research centers.

L'archive ouverte pluridisciplinaire **HAL**, est destinée au dépôt et à la diffusion de documents scientifiques de niveau recherche, publiés ou non, émanant des établissements d'enseignement et de recherche français ou étrangers, des laboratoires publics ou privés.

## RESEARCH ARTICLE

10.1002/2014JD022602

## Key Points:

- Water vapor isotopic fingerprint of Greenland summer 2012 atmospheric river
- Surface and remote sensing observations and models depict similar patterns
- Strong influence of subtropical North Atlantic moisture with low distillation

## Supporting Information:

- Text S1–S3, Figures S1–S7, and Table S1

## Correspondence to:

J.-L. Bonne,  
jean-louis.bonne@lsce.ipsl.fr

## Citation:

Bonne, J.-L., et al. (2015), The summer 2012 Greenland heat wave: In situ and remote sensing observations of water vapor isotopic composition during an atmospheric river event, *J. Geophys. Res. Atmos.*, 120, 2970–2989, doi:10.1002/2014JD022602.

Received 19 SEP 2014

Accepted 8 FEB 2015

Accepted article online 13 FEB 2015

Published online 1 APR 2015

## The summer 2012 Greenland heat wave: In situ and remote sensing observations of water vapor isotopic composition during an atmospheric river event

Jean-Louis Bonne<sup>1</sup>, Hans Christian Steen-Larsen<sup>1</sup>, Camille Risi<sup>2</sup>, Martin Werner<sup>3</sup>, Harald Sodemann<sup>4,5</sup>, Jean-Lionel Lacour<sup>6</sup>, Xavier Fettweis<sup>7</sup>, Grégory Cesana<sup>8</sup>, Marc Delmotte<sup>1</sup>, Olivier Cattani<sup>1</sup>, Paul Vallelonga<sup>9</sup>, Helle Astrid Kjær<sup>9</sup>, Cathy Clerbaux<sup>6,10</sup>, Árný Erla Sveinbjörnsdóttir<sup>11</sup>, and Valérie Masson-Delmotte<sup>1</sup>

<sup>1</sup>LSCE Laboratoire des Sciences du Climat et de l'Environnement, Gif-Sur-Yvette Cedex, France, <sup>2</sup>LMD, Paris, France, <sup>3</sup>Alfred Wegener Institute Helmholtz-Center for Polar and Marine Research Bremerhaven, Bremerhaven, Germany, <sup>4</sup>ETH Zurich, Zürich, Switzerland, <sup>5</sup>Geophysical Institute, University of Bergen, Bergen, Norway, <sup>6</sup>Spectroscopie de l'Atmosphère, Chimie Quantique et Photophysique, Université Libre de Bruxelles, Brussels, Belgium, <sup>7</sup>Department of Geography, University of Liège, Liège, Belgium, <sup>8</sup>NASA Jet Propulsion Laboratory, Pasadena, California, USA, <sup>9</sup>Centre for Ice and Climate, Niels Bohr Institute, University of Copenhagen, Copenhagen, Denmark, <sup>10</sup>Sorbonne Universités, UPMC University of Paris 06; Université Versailles St-Quentin; CNRS/INSU, LATMOS-IPSL, Paris, France, <sup>11</sup>Institute of Earth Sciences, University of Iceland, Reykjavik, Iceland

**Abstract** During 7–12 July 2012, extreme moist and warm conditions occurred over Greenland, leading to widespread surface melt. To investigate the physical processes during the atmospheric moisture transport of this event, we study the water vapor isotopic composition using surface in situ observations in Bermuda Island, South Greenland coast (Ivittuut), and northwest Greenland ice sheet (NEEM), as well as remote sensing observations (Infrared Atmospheric Sounding Interferometer (IASI) instrument on board MetOp-A), depicting propagation of similar surface and midtropospheric humidity and  $\delta D$  signals. Simulations using Lagrangian moisture source diagnostic and water tagging in a regional model showed that Greenland was affected by an atmospheric river transporting moisture from the western subtropical North Atlantic Ocean, which is coherent with observations of snow pit impurities deposited at NEEM. At Ivittuut, surface air temperature, humidity, and  $\delta D$  increases are observed. At NEEM, similar temperature increase is associated with a large and long-lasting  $\sim 100\text{‰}$   $\delta D$  enrichment and  $\sim 15\text{‰}$  deuterium excess decrease, thereby reaching Ivittuut level. We assess the simulation of this event in two isotope-enabled atmospheric general circulation models (LMDz-iso and ECHAM5-wiso). LMDz-iso correctly captures the timing of propagation for this event identified in IASI data but depict too gradual variations when compared to surface data. Both models reproduce the surface meteorological and isotopic values during the event but underestimate the background deuterium excess at NEEM. Cloud liquid water content parametrization in LMDz-iso poorly impacts the vapor isotopic composition. Our data demonstrate that during this atmospheric river event the deuterium excess signal is conserved from the moisture source to northwest Greenland.

### 1. Introduction

In summer 2012, a warm spell over Greenland led to a record extent of surface snow melt, covering 97% of the ice sheet surface during 11–12 July [Nghiem et al., 2012]. A negative North Atlantic Oscillation pattern in summer 2012 induced persistent anticyclonic conditions over Greenland, leading to melting lasting up to 2 months longer than the 1979–2011 mean in some Greenland areas, causing a decrease in the ice sheet surface mass balance reaching three standard deviations below mean value [Tedesco et al., 2013].

Other occurrences of melt episodes were observed in central Greenland ice cores over the past 10,000 years [Meese et al., 1994; Alley and Anandakrishnan, 1995]: recurrent events at a multidecadal time scale in the early Holocene (6000 to 8000 years ago) and once every about 250 years from 4000 to 1000 years ago. Several events occurred in the medieval warm period, followed by an event around year 1250. Since then, only one such event occurred in summer 1889 [Meese et al., 1994; Alley and Anandakrishnan, 1995] for which limited meteorological information is available [Neff et al., 2014].

The July 2012 event provides a unique directly observed case study to explore the atmospheric processes involved in the transport of warm and moist air masses toward Greenland and the associated feedbacks occurring in these meteorological conditions. Air mass trajectories analysis [Neff *et al.*, 2014] has evidenced that this event was triggered by the advection of dry and hot continental air from North America toward subtropical North Atlantic, initiating intense evaporation. The resulting warm and moist air was then quickly transported northward from the subtropics ahead of an advancing cold front. Greenland warming was significantly enhanced by the presence of thin low-level “liquid water” clouds (clouds containing liquid water droplets) advected from the south [Bennartz *et al.*, 2013]. While ubiquitous in the Arctic [de Boer *et al.*, 2009; Shupe *et al.*, 2006], this type of clouds is currently poorly simulated by state-of-the-art Atmospheric General Circulation Models (s), leading to biases in surface radiation [Klein *et al.*, 2009; Cesana and Chepfer, 2012; Cesana *et al.*, 2012]. Therefore, understanding the processes involved in this event may be useful to help improving the representation of extreme events in AGCMs.

The northward transport of warm and moist air during the summer 2012 event has been described as an atmospheric river [Neff *et al.*, 2014]. Atmospheric rivers correspond to filamentary structures of large water vapor transport in the troposphere [Newell *et al.*, 1992], typically on the order of magnitude of the Amazon river flux, readily identifiable by vertically integrated water vapor retrieved from satellite observations. They are responsible for more than 90% of the poleward water vapor transport in midlatitudes [Zhu and Newell, 1998], produce extreme precipitation in coastal regions, and cause mild temperatures in upper latitudes [Ralph and Dettinger, 2011; Sodemann and Stohl, 2013; Stohl *et al.*, 2008; Gorodetskaya *et al.*, 2014]. It was recently evidenced that they also provide a significant contribution to the Antarctic ice sheet surface mass balance [Gorodetskaya *et al.*, 2014]. A change of the frequency of this type of events over Greenland might lead to important climate feedbacks [Tedesco *et al.*, 2013], through effects on the ice sheet surface mass balance and albedo.

Water-stable isotopic composition provides integrated information on the evolution of atmospheric moisture and can be applied to atmospheric rivers. We focus here on H<sub>2</sub>O, H<sub>2</sub><sup>18</sup>O, and HDO water-stable isotopologues, hereafter denoted isotopes. As they have different saturation vapor pressure and diffusivity in the air, fractionation processes occur during phase changes (such as evaporation or condensation), with heavier isotopes being preferentially distributed in the condensed phase. Successive water phase changes during condensation processes caused by air mass cooling lead to a gradual depletion of the heavy isotopes in water vapor. Water isotopic compositions are commonly reported against an international scale (here Vienna SMOW (VSMOW)) in ‰ unit using the  $\delta$  notation, defined as a deviation of the sample isotopic ratio  $R$  compared to a standard isotopic ratio  $R_{\text{VSMOW}}$ :

$$\delta = 1000 \times (R/R_{\text{VSMOW}} - 1) \quad (1)$$

At the global scale, precipitation isotopic composition is distributed along the Global Meteoric Water Line [Dansgaard, 1964], identified in a  $\delta D$ - $\delta^{18}O$  diagram with a slope of 8 and an offset of 10. The second-order isotopic parameter deuterium excess, hereafter d-excess (d-excess =  $\delta D - 8 \cdot \delta^{18}O$ ), was introduced to quantify the distance to the Global Meteoric Water Line and highlight kinetic effects [Dansgaard, 1964; Craig and Gordon, 1965; Merlivat and Jouzel, 1979]. The d-excess of initial evaporated water is predominantly driven by sea surface temperature and relative humidity [Merlivat and Jouzel, 1979; Steen-Larsen *et al.*, 2014a; Pfahl and Sodemann, 2014], and this parameter should theoretically preserve a signal related to the initial moisture origin [Jouzel *et al.*, 2013; Steen-Larsen *et al.*, 2011; Bonne *et al.*, 2014; Pfahl and Sodemann, 2014]. Using d-excess to track the moisture origin is an original technique which has been applied to ice core records but seldom applied for present-day monitoring.

So far, only one atmospheric river has been investigated regarding water isotopic composition, using precipitation samples along the Californian coast. Large changes in precipitation isotopic composition were initially interpreted as the mark of different condensation heights [Copley *et al.*, 2008]. This was challenged by regional atmospheric simulations which stressed the importance of droplet reevaporation at the onset of the event followed by variations driven by horizontal advection [Yoshimura *et al.*, 2010]. This example highlights the complexity of processes affecting the isotopic composition of water during this type of events and the added value of atmospheric models to interpret isotopic variations in terms of processes.

Here we investigate moisture origins during the July 2012 atmospheric river based on observations and simulations of the water vapor isotopic composition, which opens new perspectives compared to analyses

based on precipitation sampling which are limited to rainy conditions and performed at lower frequencies. Surface water vapor isotopic composition was monitored continuously with laser-based techniques at three sites: at the potential origin of the atmospheric river [Neff *et al.*, 2014] in the Bermuda Islands [Steen-Larsen *et al.*, 2014a], in South Greenland at Ivittuut [Bonne *et al.*, 2014], and in northwest Greenland at NEEM [Steen-Larsen *et al.*, 2013, 2014b]. In South Greenland, Ivittuut measurements have previously depicted a close relationship between surface water vapor  $\delta D$  and local air temperature and humidity, at the seasonal and synoptic time scales, whereas d-excess appears to be related with relative humidity at the surface of its usual North Atlantic moisture source [Bonne *et al.*, 2014]. Both Greenland stations have revealed fingerprints of air masses origins in the water vapor isotopic composition. In particular, Arctic air masses were shown to be associated with higher d-excess values [Bonne *et al.*, 2014; Steen-Larsen *et al.*, 2013]. Water vapor with such high d-excess could be produced, predominantly during autumn and winter [Pfahl and Sodemann, 2014], when evaporation occurs with low relative humidity, leading to strong kinetic effect. This could take place in particular at the sea ice margins where dry air from areas covered with sea ice encounter open waters [Kurita, 2011]. The Bermuda Islands observations confirm the theory of Merlivat and Jouzel [1979] where d-excess of evaporated water depends on the difference between atmospheric humidity and ocean skin surface humidity. No link has been detected with wind speed or sea surface temperature [Steen-Larsen *et al.*, 2014a]. Surface measurements are completed by remote sensing observations of specific humidity and  $\delta D$  in the free troposphere above the North Atlantic performed by the Infrared Atmospheric Sounding Interferometer (IASI) on board the MetOp-A satellite [Lacour *et al.*, 2012]. Both isotopic data sets will allow to evaluate the relationships between water vapor isotopic composition and meteorological parameters (temperature, humidity) during and outside of the melt event along the moisture transport path. Surface snow pits at NEEM were sampled for impurity content before and after the melt event. The chemical composition of impurities deposited during the melt event provides additional information on air masses.

In order to investigate the atmospheric water cycle processes and the moisture source changes during the event, we use regional atmospheric models, water tagging, and moisture source diagnostic based on Lagrangian backward trajectories. We investigate if state-of-the-art AGCMs equipped with water-stable isotopes modeling and nudged to meteorological analyses can reproduce the observed isotopic signal along the atmospheric river, and we discuss the impact of cloud parametrizations on the simulated temperature, humidity, and water vapor isotopic composition.

This manuscript is organized in the following way. First, we introduce the data and methods (section 2). Results are presented in section 3: we first discuss the meteorological context, with a specific focus on the water cycle from the moisture sources and along the transport path; we then report the observed changes in water vapor isotopic composition and their representation in general circulation models. Our conclusions are given in section 4.

## 2. Data and Methods

Throughout the manuscript, we will use the notations  $T$ ,  $q$ , and RH, respectively, for air temperature, specific humidity, and relative humidity.

### 2.1. In Situ Water Vapor Isotopic Measurements

This study is based on in situ observations of surface water vapor isotopic composition performed at two Greenland sites and in Bermuda Islands, using continuous laser-based analyzers. Two types of analyzers have been used at these stations: WS-CRDS (Wavelength Scanned Cavity Ring-Down Spectrometry) or OA-ICOS (Off-Axis Integrated Cavity Output Spectroscopy). These instruments have been operated semi-autonomously and are calibrated against the VSMOW scale using different liquid water standards.

Ivittuut is a coastal South Greenland site (61.2°N, 48.17°W, altitude 30 m above sea level (asl)) where several instruments have been deployed for the autonomous monitoring of atmospheric composition. A Picarro Inc. WS-CRDS analyzer (product number L2120-i) has been deployed on site from September 2011 to September 2014, with an inlet located at about 5 m above ground level (agl). Meteorological parameters ( $T$ , RH, air pressure, and wind speed and direction) have also been measured in the station as well as in Grønnedal, 5 km east from Ivittuut. Temperature observations presented here are based on observations from both sites. Further details on the water vapor isotopic composition and meteorological monitoring methods are given in Bonne *et al.* [2014].

The NEEM camp was established on the ice sheet in northwest Greenland (77.45°N, 51.05°W; 2484 m asl) for drilling Greenland oldest ice [NEEM-Community-Members, 2013]. In order to understand the processes controlling the isotopic composition of surface snow, continuous measurements of water vapor isotopic composition were performed during four summer field campaigns. Cold trap sampling provided first discrete measurements in 2008 [Steen-Larsen *et al.*, 2011]. During three successive summer campaigns, from 2010 to 2012, WS-CRDS and OA-ICOS (Off-Axis Integrated Cavity Output Spectroscopy) instruments were deployed and provided continuous records of surface water vapor isotopic composition in 2010 [Steen-Larsen *et al.*, 2013], 2011, and 2012 [Steen-Larsen *et al.*, 2014b]. During the summer 2012 melt event, water vapor isotopic composition was monitored on site by a Picarro Inc. WS-CRDS analyzer (product number L1102-i). Two inlet levels were located at 3 m and 20 cm height. Alternate measurements of the 3 m and 20 cm levels were performed, respectively, for 45 and 15 min every hour. Here we only use the measurements performed at 3 m height. Meteorological measurements have also been performed (measuring  $T$ , RH, air pressure, and wind speed and direction). Further details on the water vapor isotopic composition and meteorological monitoring methods are given in Steen-Larsen *et al.* [2014b].

Bermuda observations have been performed at the Tudor Hill Atmospheric Observatory in Bermuda (32.26°N, 64.88°W) since November 2011, on a meteorological tower situated  $\sim 30$  m inland from the coast, where meteorological parameters are also recorded ( $T$ , RH, air pressure, and wind speed and direction). Water vapor isotopic composition was monitored on site by a Picarro Inc. (Model HBDS-2120) WS-CRDS analyzer. Inlets were located on the tower at  $\sim 49$  m asl. Further details on the water vapor isotopic composition and meteorological monitoring methods are given in Steen-Larsen *et al.* [2014a].

The instrumental accuracies and precisions have been evaluated, respectively, for  $\delta D$  and d-excess at 2.2‰ and 4.9‰ for Ivittuut [Bonne *et al.*, 2014], at 1.4‰ and 2.3‰ for NEEM [Steen-Larsen *et al.*, 2013], and at 0.85‰ and 1.1‰ for Bermuda [Steen-Larsen *et al.*, 2014a]. We will also use the surface  $T$  and RH values provided by meteorological instruments at each site.

## 2.2. IASI Remote Sensing Data and Model-Data Comparison Methodology

In this study, we use remote sensing observations from the IASI instrument on board the MetOp-A satellite to provide vertically integrated estimates of both atmospheric water vapor content and  $\delta D$  ratios in water vapor. Water vapor content and  $\delta D$  were inferred from IASI radiance spectra following the method described in Lacour *et al.* [2012]. IASI observations are restricted to clear sky areas and cannot be exploited over continental surfaces in this study due to the difficulty of the sounder to get reliable information over ice. The IASI observations are vertically integrated between 3.5 and 6.5 km, as the instrument sensitivity peaks at these altitudes. It is therefore difficult to compare it directly with in situ measurements at the surface. The  $\delta D$  observational error for the 3–6 km layer has been estimated to be 38‰ on an individual observation [Lacour *et al.*, 2012]. This error is lowered when averaging several observations. Here IASI observations have been horizontally regridded on the LMDz-iso model grid (see section 2.4) in order to facilitate the model-data comparison. IASI retrievals have also been a posteriori corrected to provide an optimal combined use of water vapor content and  $\delta D$  [Schneider *et al.*, 2012], as in Pommier *et al.* [2014].

## 2.3. Distillation Simulation Using a Theoretical Model

The most simple modeling approach to understand the evolution of the water vapor isotopic composition between Ivittuut and NEEM relies here on the use of the mixed cloud Rayleigh distillation model Mixed Cloud Isotopic Model (MCIM), introduced by Ciais and Jouzel [1994] and already applied for NEEM ice core water isotopes [Steen-Larsen *et al.*, 2011]. Assuming that the surface isotopic composition and temperature are representative of condensation conditions, we use the Ivittuut data (surface  $T$ , air pressure, RH, and water vapor isotopic composition) at the time of the local  $q$  maximum (identified as the time of the atmospheric river) as a starting point for distillation calculations and NEEM data (surface  $T$  and pressure) at the beginning of the warm period to estimate the final condensation characteristics. This calculation assumes that Ivittuut moisture is the only moisture source for NEEM. The same calculation has also been performed using the average summer Ivittuut and NEEM conditions.

This simulation is to be interpreted with caution, as the fast variations of Ivittuut conditions during the event (decorrelated  $q$  and  $T$  maxima, associated with fast changes in water vapor isotopic composition) creates an ambiguity in the values which should be compared to those at NEEM.

#### 2.4. Isotopic Enabled Atmospheric General Circulation Models

In order to investigate whether Atmospheric General Circulation Models (AGCMs) can reproduce the main features of the observed atmospheric river and the associated changes in water vapor isotopic composition, we use here simulations performed with two AGCMs (LMDz-iso and ECHAM5-wiso) including water-stable isotopes modeling. In these models, the water-stable isotopes are introduced in atmospheric models by replacing the variables representing water by a set of variables representing each isotope (e.g.,  $\text{H}_2^{16}\text{O}$ ,  $\text{H}_2^{18}\text{O}$ , and HDO). All isotopes are passively transported and undergo fractionation during phase changes. For both simulations, large-scale dynamics are nudged to atmospheric reanalyses, but the hydrological cycle and the water isotopic composition is freely modeled by the physics of each atmospheric model.

##### 2.4.1. LMDz-iso Model

The isotope-enabled version of LMDZ4 [Hourdin *et al.*, 2006], LMDz-iso, has been developed at the Laboratoire de Météorologie Dynamique (LMD) by Risi *et al.* [2010]. The model has a uniform horizontal resolution of  $3.75^\circ$  in longitude and  $2.5^\circ$  in latitude and 19 vertical levels. The simulation used here was performed using monthly observed sea surface temperature (SST) and sea ice cover and nudged to 6-hourly three-dimensional wind fields derived from the European Centre for Medium-Range Weather Forecasts (ECMWF) operational analyses [Dee *et al.*, 2011; Rabier *et al.*, 2000], which drives a realistic synoptic variability. Daily outputs from the lowermost model layer are used for the comparison with Ivittuut, NEEM and Bermuda in situ observations. The top of this bottom model layer is located in Greenland about 20 hPa above the ground. We use LMDz-iso model outputs from the grid cells centered at the location of the measurement sites:  $62.11^\circ\text{N}$ ,  $48.75^\circ\text{W}$  for Ivittuut,  $77.32^\circ\text{N}$ ,  $52.5^\circ\text{W}$  for NEEM and  $31.69^\circ\text{N}$ ,  $63.75^\circ\text{W}$  for the Bermuda Islands.

In order to perform model-data comparisons with IASI remote sensing observations, LMDz-iso simulations have been extracted on the same vertical layer as IASI observations. Because  $\delta D$  observations from IASI contain a certain amount of a priori information and have limited vertical sensitivity, the comparison with LMDz-iso makes more sense when smoothing model vertical profiles with the averaging kernels of the IASI retrieval (sensitivity matrices of the retrieval). By doing so, the model outputs consider the same part of the atmosphere as IASI and with the same content of a priori information.

In both Ivittuut and NEEM [Bonne *et al.*, 2014], LMDz-iso is able to reproduce the timing of observed variations in surface water vapor  $\delta D$  at the interannual to intraseasonal time scales. However, it shows significant biases in both sites, with too cold and dry air associated with overdepleted precipitation and surface vapor at Ivittuut, and oppositely too warm and wet air and enriched precipitation and surface vapor at NEEM. At Ivittuut, the observed amplitude of variations is in between those simulated at the nearest ice sheet grid cell and at the nearest oceanic grid cell (respectively producing too large and too small variations), as the station is at the interface of ocean and ice sheet and the model spatial resolution is relatively low. The model also underestimates the amplitude of  $\delta D$  variations at NEEM. LMDz-iso has been shown to strongly underestimate the d-excess synoptic variations in NEEM and its synoptic and seasonal variations in Ivittuut. The stronger relationship between North Atlantic surface RH and Ivittuut observed d-excess compared to simulated Ivittuut d-excess suggests an underestimation of d-excess conservation during transport in the model.

##### 2.4.2. ECHAM5-wiso Model

The ECHAM5-wiso AGCM [Werner *et al.*, 2011] is the isotope-enabled version of ECHAM5 [Roeckner *et al.*, 2006]. We have used here a simulation performed at the spectral resolution T63, corresponding to an horizontal grid of  $1.9^\circ$  by  $1.9^\circ$ , and a vertical resolution of 31 levels. ECHAM5-wiso is also nudged to 6-hourly ECMWF analyses using pressure, temperature, divergence, and vorticity [Rast *et al.*, 2013]. This nudging method is therefore stronger than for LMDz-iso, due to the use of the temperature constraint. For the comparison with Ivittuut and NEEM surface data, we use the ECHAM5-wiso model outputs from the nearest grid cells:  $60.62^\circ\text{N}$ ,  $48.75^\circ\text{W}$  for Ivittuut and  $77.41^\circ\text{N}$ ,  $50.63^\circ\text{W}$  for NEEM. Here the coordinates represent the center of the grid cells. Contrary to LMDz-iso model, the diagnostic of estimate of IASI retrievals in the model is not implemented in ECHAM5-wiso.

To our knowledge, no evaluation of ECHAM5-wiso over Greenland has been published yet. However, in an evaluation of the previous model release ECHAM4-iso over Greenland, a warm bias has been depicted over the ice sheet, probably associated with model biases for surface temperature inversion or albedo [Sjølte *et al.*, 2011; Werner and Heimann, 2002].

## 2.5. Regional Atmospheric Modeling

### 2.5.1. MAR Model

Modèle Atmosphérique Régional (MAR) is a regional climate model coupled to the 1-D Surface Vegetation Atmosphere Transfer scheme SISVAT (Soil Ice Snow Vegetation Atmosphere Transfer). The atmospheric part of MAR is fully described in *Gallée and Schayes* [1994], while the SISVAT scheme is detailed in *De Ridder and Gallée* [1998]. MAR has been specifically developed for the polar regions and has been intensively validated over the Greenland Ice sheet [*Fettweis et al.*, 2013], particularly for the simulation of the Greenland ice sheet surface mass balance [*Fettweis et al.*, 2011]. It correctly captures the summer 2012 exceptional melt extent and duration [*Tedesco et al.*, 2013].

The MAR setup used here is at a spatial resolution of 25 km, an integration domain of 2000 km  $\times$  3500 km centered on Greenland and 23 vertical levels from 3 m to 15 km with seven levels below 100 m. The ERA-40 analyses (1957–1978) and after that the ERA-Interim analyses (1979–2013) from the ECMWF are used to initialize the meteorological fields at the beginning of the simulation in September 1957 and to force the lateral boundaries with  $T$ ,  $q$ , and wind components at each vertical level of MAR during the simulation. The 6-hourly wind fields from reanalyses are also used to force the upper boundary (above the tropopause) of MAR over the whole integration domain. Finally, the SST and the sea ice extent are also prescribed into MAR.

### 2.5.2. Water Tagging in CHRM Model

In order to identify the atmospheric river moisture sources, we use the Climate High Resolution Model (CHRM) regional atmospheric model [*Sodemann et al.*, 2009] as the water tagging method is implemented in this model. This method consists in introducing dye in the model hydrological cycle: the water is marked by its origin with a tag or label, and the tags are redistributed with water during phase changes. CHRM has mostly been used to simulate climate in the midlatitudes [*Vidale et al.*, 2003] and in contrast to MAR does not contain special adjustments to high-latitude processes. The CHRM simulation setup is similar to the setup described by *Sodemann and Stohl* [2013] for the diagnostic of moisture origins during an atmospheric river over western Scandinavia. The description of the tagging method is given in *Sodemann et al.* [2009].

The model has been run for a large North Atlantic domain encompassing Greenland and Europe (see the tracers location in *Sodemann and Stohl* [2013, Figure 1]). The model has a  $0.5^\circ \times 0.5^\circ$  horizontal resolution, with 40 vertical levels. As shown in Figure 4a, the tracers (or tags) were initialized from  $10^\circ$  latitudinal bands over the North Atlantic, from the land (representing one single moisture source) and from moisture entering the domain from the southern, western, and northeastern boundaries [*Sodemann and Stohl*, 2013]. The simulation is initialized from operational ECMWF analyses at a spectral resolution of T799 and 91 vertical levels and interpolated onto a  $1^\circ \times 1^\circ$  horizontal grid spacing. Wind fields were nudged to ECMWF atmospheric reanalyses throughout the simulation. In a spin-up period from 1 to 15 June 2012, a stronger nudging coefficient was employed to obtain a well-defined initial state for the meteorological situation while allowing moisture with undefined origin to leave the domain. Thereafter, the nudging coefficient was decreased by 1 order of magnitude to allow for a more free evolution of the meteorological conditions in the domain. Throughout this latter period, typically about 98% of the water vapor in the model domain belongs to identified sources. At the location of both stations, we extract the fraction of each source region tracer contributing to the vertically integrated water vapor in the lower troposphere (below 600 hPa).

## 2.6. Moisture Source Diagnostic

In order to analyze moisture origins, we use a moisture source diagnostic based on Lagrangian backward trajectories [*Sodemann et al.*, 2008]. Backward trajectories are computed using the FLEXPART model version 8.1 [*Stohl et al.*, 2005], following the ECMWF ERA-Interim reanalyses at  $1^\circ$  horizontal resolution and 60 vertical levels [*Dee et al.*, 2011]. Air parcels are traced 10 days backward in time from a box over NEEM ( $77.50^\circ\text{N}$ ,  $51.60^\circ\text{W}$  to  $77.90^\circ\text{N}$ ,  $50.60^\circ\text{W}$  and from 2400 to 2900 m asl). Variations of  $q$  along the air masses trajectories from one time step to the next are interpreted as moisture being taken up or released between both time steps (see *Sodemann et al.* [2008] for further details). Multiple outputs are computed on a global  $1^\circ \times 1^\circ$  grid. The locations of moisture uptakes and loss contributing to NEEM moisture are given by the integration of all moisture uptakes and loss occurring along the multiple trajectories projected on this grid. Integrated uptakes are differentiated depending on the location within or above the boundary layer, respectively called “moisture uptake in the boundary layer” and “moisture uptake in the free troposphere.” Both quantities are reported in millimeter per day (mm/d), representing the height of liquid water column added each day in the air masses over the grid cell area. The difference between gain and loss of water

along the trajectories integrated over the multiple trajectories and projected on the output grid provides an estimate of the locations where air masses predominantly gain or lose water during transport. This parameter, called “evaporation-precipitation,” is expressed in millimeters per day. If this quantity is positive (negative), the air masses predominantly gain (lose) water in this area. The integrated quantity of water transported along the multiple trajectories (taking into account all gain and loss of water along trajectories) is an estimate of the total amount of water present in the air masses advected to NEEM. This parameter, hereafter called “moisture transport,” is reported in millimeters (mm) representing the corresponding height of the liquid water column contained in the grid cell that is then going to NEEM, integrated over the particles lifetime (here 10 days). This methodology is here employed to map the origins of NEEM moisture, following the same procedure as described in *Bonne et al.* [2014] for Ivittuut moisture source identification. Ivittuut moisture source identification results for this event are also presented in supporting information Figure S1.

### 2.7. Time Scales Used for the Analyses

For the interpretation of all data sets, we used two different averaging time steps. The analyses of meteorological observations (section 3.1) and water vapor isotopes in situ measurements (section 3.3) are based on observations with a step of 6 h averaged over 30 min. The comparison of model outputs (MAR model in section 3.1, moisture transport models in section 3.2, and AGCMs in section 3.5) and remote sensing observations with in situ observations (section 3.3) are based on daily averages.

## 3. Results and Discussion

### 3.1. Greenland Meteorological Changes During the Melt Event

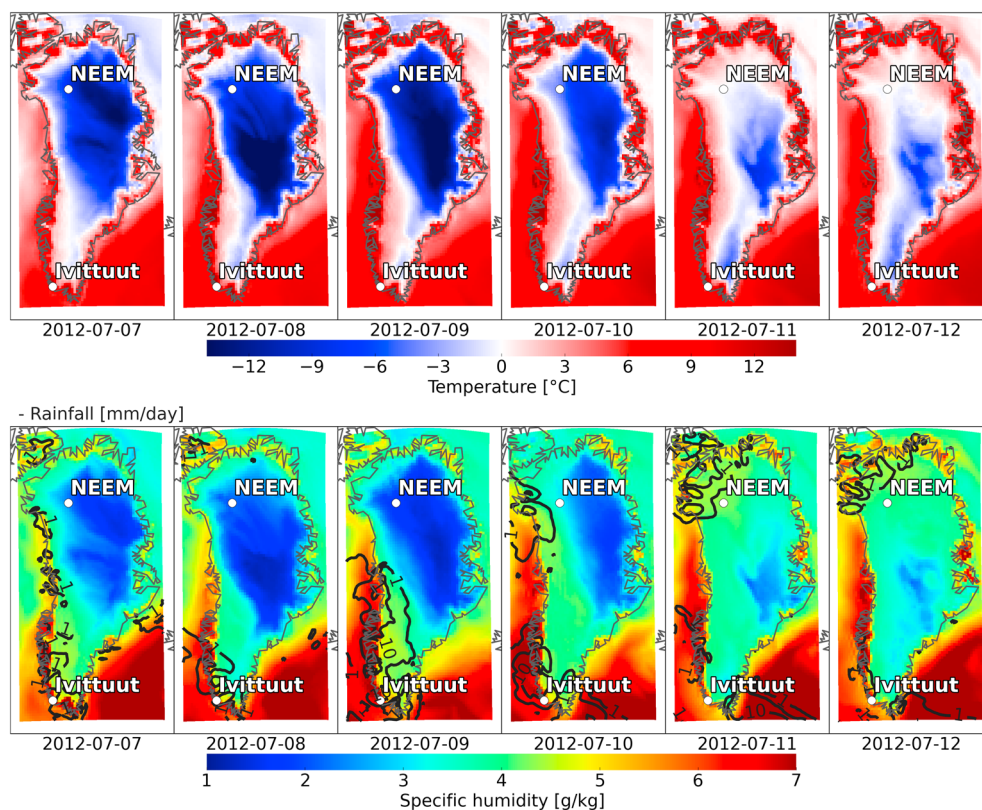
We first look at the meteorological situation, depicted by the regional model MAR and by surface observations at Ivittuut and NEEM. This allows us to diagnose the timing of air masses arrival in both Greenland stations and to quantify the meteorological changes ( $T$ ,  $q$ , and precipitations) occurring during the melt event.

Figure 1 displays the daily evolution of  $T$ ,  $q$ , and precipitation over Greenland, as simulated in the model first vertical level of MAR (2–3 m agl), from 7 July to 12 July 2012. On 8 July, a moist air mass arrives over the southwest coast of Greenland. This air mass then moves northward along the Greenland west coast on 9 July and 10 July. Precipitation occurs along this path, mostly over the southwest coast of Greenland (probably driven by the Greenland coast topography). The wet air mass then shifts eastward and is lifted onto the Greenland ice sheet on 11 July. It progressively expands over the whole Greenland ice sheet, where surface  $q$  values increase (for example in NEEM from about 2 g/kg on 8 July to about 4 g/kg on 12 July).

At Ivittuut, surface air  $T$  increases by about 10°C from 8 July to 9 July and reaches peak values of 21.1°C at 21 h UTC on 9 July (Figure 2a). Ivittuut  $q$  increases from 6 to maximum values of 11 g/kg observed on 8 July at 21 h UTC (Figure 2b), therefore 1 day earlier than peak  $T$ . Both  $T$  and  $q$  anomalies last altogether 2 days. The  $q$  levels then decrease and reach background levels on 10 July. CALIPSO data (see supporting information Text S1) show enhanced high-altitude cloudiness over Ivittuut between 8 and 10 July. This observation is supported by the MAR simulated cloud cover, presenting few episodic clouds over Ivittuut on 8 July and a large cloud cover on 9 and 10 July which moves eastward on the ice sheet on 11 July. This suggests that the lag between the  $T$  and  $q$  maxima might be linked with the radiative effect of clouds, but this hypothesis needs further analysis, e.g., on the different types of clouds (compositions and altitude) and on their radiative forcing. The importance of cloud positive radiative feedback has also been highlighted at Summit on top of the ice sheet during the atmospheric river event [*Bennartz et al.*, 2013]. We note that the  $T$  and  $q$  increases at Ivittuut reach larger magnitudes than the other synoptic events encountered year round (on average +7°C, ~+2.5 g/kg) [*Bonne et al.*, 2014].

At NEEM (Figures 2a and 2b),  $T$  and  $q$  simultaneously sharply increase within 12 h. On 10 July, surface air  $T$  shifts from -10.3°C at 6 h UTC to +0.5°C at 18 h UTC. In parallel, surface  $q$  has a more than twofold increase from ~1.5 to ~4 g/kg. From 10 July at 18 h UTC to 15 July at 00 h UTC, surface air temperature stays above -1°C and even reaches +2.9°C on 14 July at 18 h UTC.  $T$  and  $q$  values gradually decrease after 16 July and reach background levels around 19 July. In summary, we observe the same amplitude of  $T$  anomaly (10°C) in South and northwest Greenland. The amplitudes of  $q$  increases are on the same order of magnitude in Ivittuut and NEEM, but the duration of the event is longer above the ice sheet than on the southern coast.

Another high  $T$  maximum is observed between 27 and 29 July 2012 but with a relatively lower importance in terms of Greenland ice sheet melting [*Tedesco et al.*, 2013]. We again observe a lag between  $T$  and  $q$  spikes in



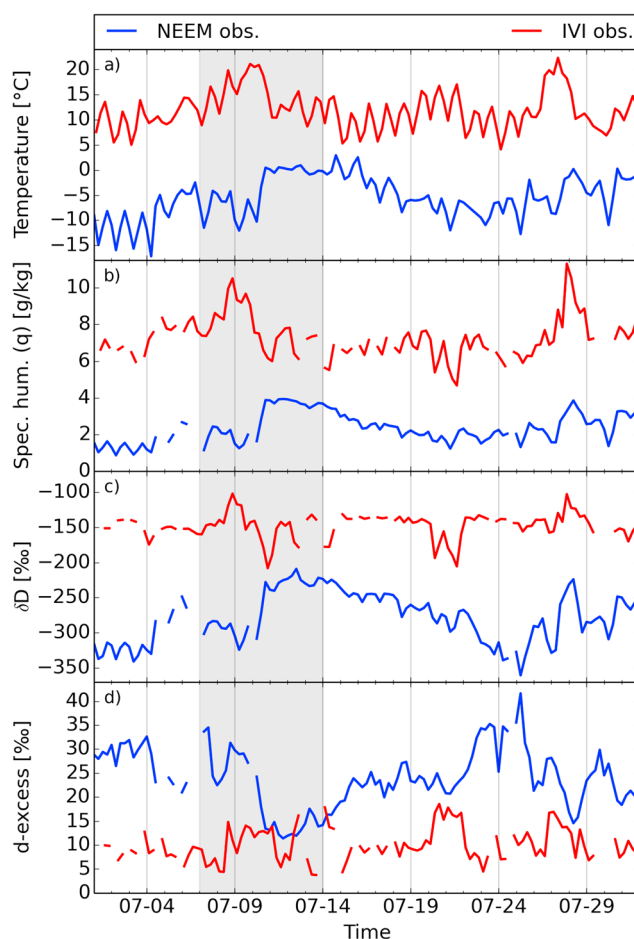
**Figure 1.** Simulated daily mean surface temperature (top color maps), specific humidity (bottom color maps, in g/kg), and precipitation (black curves on bottom maps, in mm/day) from MAR regional model outputs at the first model vertical level (2–3 m agl), from 7 to 12 July 2012.

Ivittuut, but in this case, the  $q$  maximum occurs after the  $T$  maximum. In NEEM,  $T$  and  $q$  increase are almost as important as for the first event, but the perturbation is much shorter and lasts about 1 day.

### 3.2. Moisture Sources Locations

We now investigate the origins of moisture contributing to the atmospheric river event. Backward trajectory simulations of air masses have already been performed by *Neff et al.* [2014] for Summit in central Greenland. Here we use the moisture source diagnostic based on Lagrangian backward trajectories to gain information on the uptakes and outtakes of moisture during air masses transport. Outputs from the regional model CHRM also provide a quantification of the relative contributions of different moisture sources without the constraints of backward trajectory lifetime, taking into account the integrated water gains and losses along transport and with thinner horizontal resolution. Results from atmospheric moisture transports are finally coherent with direct observations of snow pits impurities performed in NEEM.

The atmospheric circulation has been described during the event by *Neff et al.* [2014], showing that this period was characterized by an abrupt change in the Arctic atmospheric circulation. The Arctic Oscillation (AO) transited from a negative to a positive phase between 5 July and 12 July 2012, potentially creating an opportunity for northward transport of heat and moisture. On 9 July 2012, a cyclonic circulation was centered over the coast of Newfoundland, whereas an anticyclonic circulation was centered over the southeast coast of Greenland, leading to northward winds along the west coast of Greenland. *Neff et al.* [2014] also noted that the Atlantic Multidecadal Oscillation (AMO) was in its positive phase during June and July 2012 and may have enhanced the warm and wet anomaly, as it led to 2°C positive SST anomalies just south of Greenland. This large-scale atmospheric and oceanic situation allowed the atmospheric transport of air masses from North America over subtropical North Atlantic where intense evaporation could take place; these warm and wet air masses subsequently shifted northward to Greenland [*Neff et al.*, 2014]. We will now analyze the atmospheric transport of moisture in these air masses.



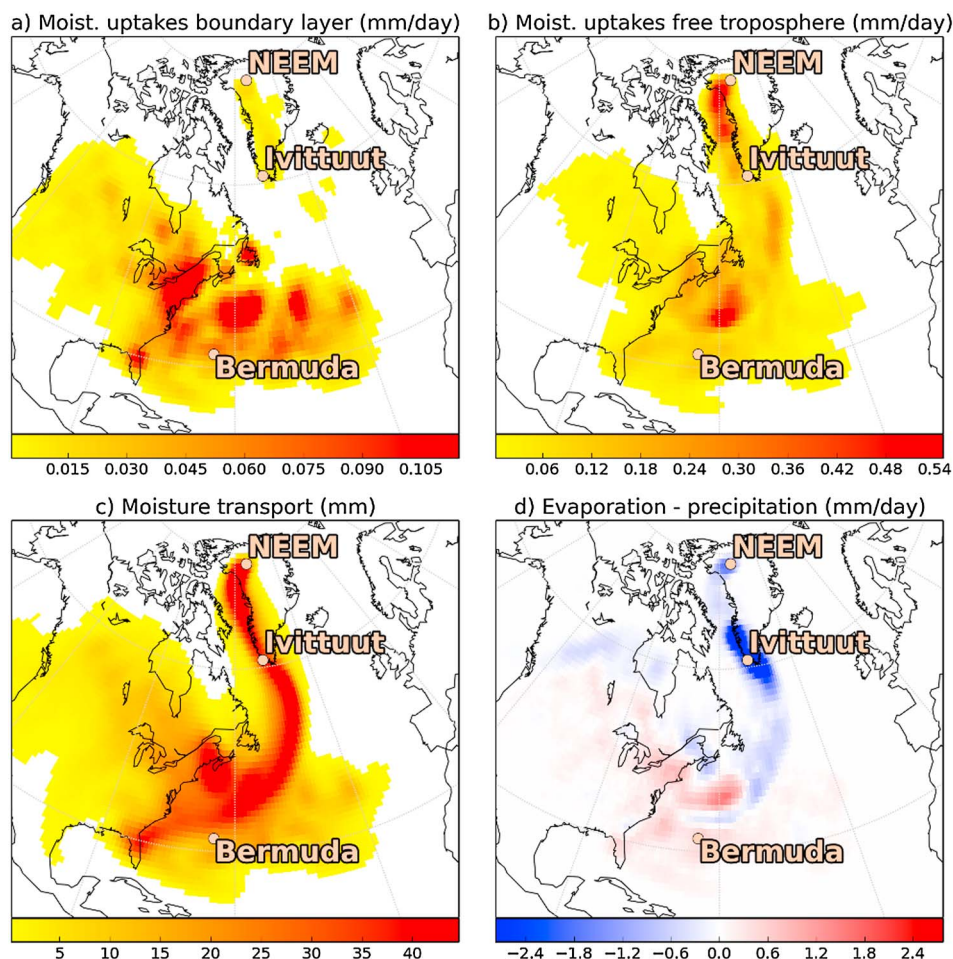
**Figure 2.** Observations averaged over 30 min every 6 h at Ivittuut (IVI, red) and NEEM (blue) of (a) temperature (°C), (b) specific humidity (g/kg), (c)  $\delta D$  (‰), and (d) d-excess (‰), from 1 July to 31 July 2012. Temperature observations from Ivittuut are an average of Ivittuut and Grønnedal (5 km west of Ivittuut) observations. The gray-shaded rectangle represents the atmospheric river event.

Figure 3 presents the results from the moisture source diagnostic, for water vapor arriving at NEEM on 11 July 2012. The main areas of evaporation contributing to NEEM moisture (boundary layer uptakes) is located over the subtropical North Atlantic (see Figure 3a), off the North American east coast (over the northern part of the Sargasso Sea and the Gulf Stream zone). This moisture is advected northward following a narrow band reaching southern Greenland (Figure 3c) and the surroundings of Ivittuut, which is confirmed by moisture source diagnostic for Ivittuut (see supporting information Figure S1). This moist air mass then moves northward along the western Greenland coast, before shifting eastward toward northwest Greenland and reaching NEEM on 11 July. During the northward transport path over the Davis strait and Baffin Bay area, our calculations depict an important moisture uptake in the free troposphere, up to 3 times larger than the initial boundary layer uptake (Figure 3b). Based on the coincidence with local precipitation simulated by MAR (Figure 1) and the moisture source diagnostic analyses (Figure 3d), we suggest that this free-tropospheric moistening may arise either from detrainment of boundary layer air due to convective processes or from precipitation evaporation. The oceanic

area providing most moisture uptake inside the boundary layer is located at the southern part of usual moisture sources for Ivittuut high-humidity synoptic events [Bonne et al., 2014].

During the second event at the end of July, our analyses show moisture sources in NEEM similar to those during the first event but with more intense precipitation between Ivittuut and NEEM (not shown).

The attributions of integrated water vapor at Ivittuut and NEEM to different moisture sources, calculated from the decomposition of the total water vapor into contribution from the tagged water tracers using CHRM regional model, are presented in Figure 4b. The small fraction of water vapor not assigned to any tracer is due to numerical diffusion and numerical inconsistencies [Sodemann and Stohl, 2013]. For both stations, prior to the melt event, summer moisture mostly originates from land evapotranspiration (gray), followed by a western boundary tracer (mainly North American continent). This is consistent with intense continental recycling in summer and with earlier moisture source diagnostic depicting a dominant contribution to Ivittuut moisture during summer from the northeastern American continent and South Greenland [Bonne et al., 2014]. NEEM receives a larger fraction of moisture from northeastern boundaries, while Ivittuut is diagnosed to receive a larger fraction of nearby sources (50–70°S, T4 and T5, red and purple). The contribution of this region to Ivittuut moisture has been independently suggested by the correlation between Ivittuut d-excess intraseasonal variability and North Atlantic surface RH [Bonne et al., 2014]. The melt event is associated with a major change in moisture origin, identified from 8 to 9 July at Ivittuut and 11 to 14 July at NEEM, marked by a dramatic reduction of the proportion of land surface



**Figure 3.** Map of moisture sources and transport to NEEM identified from the Lagrangian moisture source diagnostic on 11 July 2012. (a) Moisture uptake inside boundary layer (mm/day); (b) moisture uptake in the free troposphere (mm/day); (c) moisture transport (mm); and (d) evaporation minus precipitation (mm/day). Dots show the positions of NEEM, Ivittuut, and Bermuda.

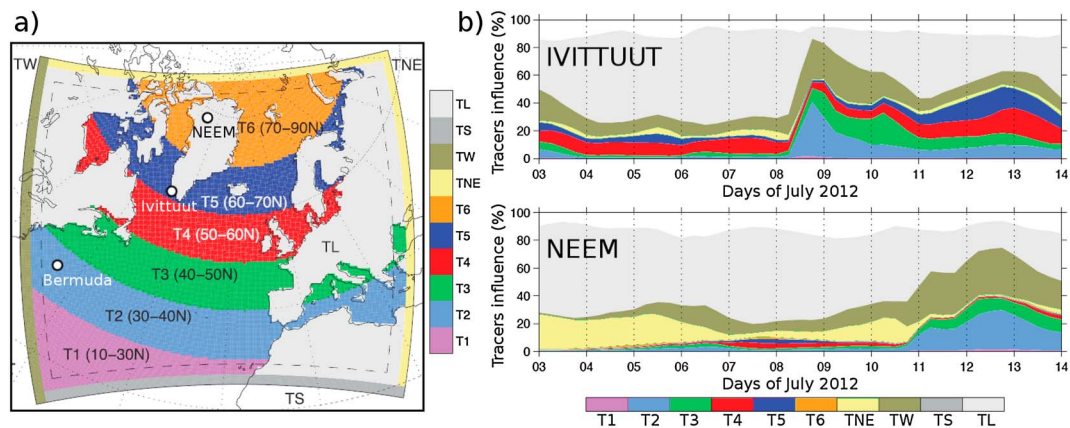


**Figure 4.** (a) Calculation domain of the CHRM model (solid black line) and interior model domain (dashed black line), figure adapted from Sodemann and Stohl [2013] (©American Meteorological Society; used with permission). Colors show water vapor tracers released by surface evaporation from every 10° latitude band of ocean area (T1 to T6), from land (TL, here plotted in white), and from advection through the southern (TS), western (TW), and northeastern (TNE) boundaries reaching from the bottom to top of the model domain. Initial atmospheric tracer (TA) is not displayed. (b) Time series of the simulated relative proportion (%) of the different tracers in the lower troposphere (below 600 hPa) for the two Greenland sites during 3–14 July 2012.

moisture source (from ~65 to ~10% in Ivittuut and from ~55 to ~20% in NEEM) and a major increase in the contribution of moisture from the subtropical Atlantic (T2, 30–40°N, blue tracer, from ~2 to ~40% in Ivittuut and from ~2 to ~30% in NEEM) and, second, the nearby oceanic regions (T3, 40–50°N, green tracer, from ~4 to ~10% in Ivittuut and from ~2 to ~10% in NEEM).

To further characterize the moisture source leading to the Greenland melt event, we investigated impurities in snow pits at NEEM prior to and after the melt event (see supporting information Text S3). These data reveal a sevenfold increase of sodium ( $\text{Na}^+$ ) concentrations following the melt event (Table S1 and Figure S7 in the supporting information). Such high levels of sea salts are unusual for high-altitude inland sites and have not been observed in the NEEM deep ice core record covering the entire current interglacial period (the Holocene). These results suggest that the precipitation which occurred during the melt event originated from an air mass unusually enriched in sea salts. This is consistent with the moisture uptake that occurs with strong convective updraft.

### 3.3. Observations of Water Vapor Isotopic Composition

Different moisture sources have been depicted for the background summer conditions and for the melt event period. The isotopic composition of water should reflect these distinct moisture sources. We use here the surface-based observations as well as satellite remote sensing observations of water vapor isotopic composition to track the propagation of an isotopic signal associated with this atmospheric river event.

The time series of Ivittuut and NEEM surface water vapor isotopic observations are shown in Figures 2c and 2d. Before the melt event, they display a north-south isotopic gradient, as expected from air mass distillation, with 150‰ to 200‰ more depleted  $\delta D$  values at NEEM compared to Ivittuut. The isotopic gradient is also marked by a much higher level of d-excess at NEEM (20‰ above Ivittuut level). The poleward increase in water vapor d-excess possibly results from the impact of cold temperatures on fractionation. It is also expected to vary if NEEM receives either more moisture from the low latitudes (warmer moisture source) and/or more moisture from the Arctic. Indeed, moisture formed at the sea ice margin, where kinetic effects are expected to be strong, would have a high d-excess [Kurita, 2011; Steen-Larsen et al., 2013].

The isotopic signal at Ivittuut shows a +6‰ d-excess increase occurring between 9 July at 09 h and 10 July at 21 h UTC. The  $\delta D$  data depict a brief 46‰ enrichment on 8 July, followed by a fast decrease on 10 July. The  $\delta D$  maximum occurs in phase with the local  $q$  spike (see section 3.1), but earlier than the  $T$  maximum. This  $\delta D$  maximum corresponds to the highest recorded  $\delta D$  value in Ivittuut measurements, about 50‰ higher than usual summer 2012 and 2013 values [see Bonne et al., 2014, Figure 5]. The  $\delta D$  local minimum following the  $\delta D$  maximum is reached when  $T$  is still high and begins to decrease. At Ivittuut,  $\delta D$  variations are similar to usual synoptic variations but coincide with a d-excess increase. This contrasts with the anticorrelation between d-excess and  $\delta D$  during synoptic events [Bonne et al., 2014]. During the few days before this event, Ivittuut moisture sources (not presented) are already located southwest of Greenland, and the melt event corresponds to moisture sources located unusually further south. During common synoptic events, the antiphase of d-excess and  $\delta D$  indeed reflects the shifts between Arctic sources prior to the events and Atlantic sources during the storm events. We stress that the parallel increase of  $\delta D$  and d-excess of surface vapor is therefore a good indicator of subtropical moisture inflow.

Two days later, the atmospheric river reaches NEEM where it produces large and long-lasting variations.  $T$ ,  $q$ ,  $\delta D$ , and d-excess changes (respectively +10°C, +2.5 g/kg, +75‰, and –15‰) occur very abruptly within 12 h on 10 July and simultaneously, contrary to the observations at Ivittuut. Ivittuut station is located next to a fjord a few kilometers from both the ice sheet and the Labrador Sea. As a result, local water vapor might reflect a more complex set of influences than in NEEM, over the ice sheet. At NEEM, the recovery during the days after the event (from 14 July to 21 July 2012) is progressive for  $\delta D$  and meteorological parameters. We note that this recovery is more stepwise for d-excess than for the other parameters, possibly as a result of changes in moisture origin, while other parameters may be more strongly affected by local feedbacks associated with surface snow-air interactions and/or cloud radiative feedbacks. During the event, the d-excess gradient between Ivittuut and NEEM is reduced from 20‰ to less than 5‰. This reduced d-excess gradient is consistent with a similar moisture source affecting first southern then northern Greenland.

At NEEM, the  $\delta D/T$ ,  $\delta D/q$ , d-excess/ $T$ , d-excess/ $q$ , and d-excess/ $\delta D$  relationships during the event are similar with the same relationships during the rest of the summer 2012 period (see supporting information Figure S2).

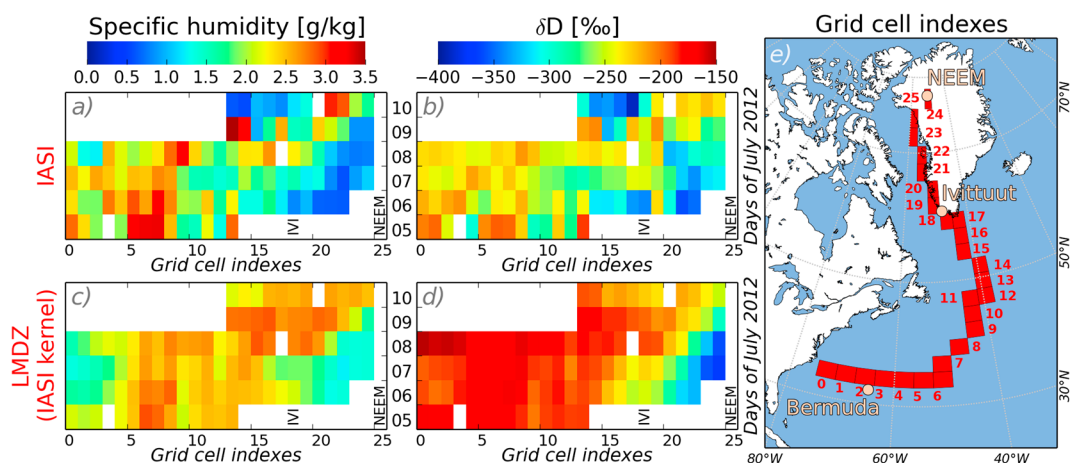


**Figure 5.** (a to d) IASI and LMDz-iso specific humidity (g/kg) and  $\delta D$  (‰) daily averaged data along a series of grid cells, presented in Figure 5e, following the air mass trajectory from the North Atlantic to NEEM, from 5 to 11 July 2012. Data are vertically integrated between 3.5 and 6.5 km. The horizontal axes represent the grid cell indexes as noted on the map from Figure 5e, and the vertical axes represent the time (in days of July 2012). Specific humidity observed by IASI (Figure 5a);  $\delta D$  observed by IASI (Figure 5b); specific humidity simulated by LMDz-iso smoothed with IASI kernel (Figure 5c); and  $\delta D$  simulated by LMDz-iso smoothed with IASI kernel (Figure 5d). (e) Grid cells where data of Figures 5a–5d are extracted, with their index number.

The second event at the end of July shows strong similarities in the surface isotopic measurements. It has a weaker fingerprint in meteorological data (particularly concerning the event duration at NEEM). Concerning the water vapor isotopic composition, we note that similarly enriched values are observed at Ivittuut (close to  $-100$ ‰ in  $\delta D$ ), associated with comparable d-excess variations. At NEEM, this second event displays an increase in  $\delta D$  and a decrease in d-excess. However, the fast change of air masses origins associated with more intense precipitation occurring between Ivittuut and NEEM probably explains the reduced amplitude of  $\delta D$  and d-excess spikes at NEEM.

Using IASI retrievals, we have also extracted the evolution of the atmospheric integrated vapor isotopic composition between 3.5 and 6.5 km above ground level, for a series of grid boxes located along the moisture transport path (Figure 5e). As seen in Figures 5a and 5b, we detect the progression of the atmospheric river with the same timing as in surface observations. The  $\delta D$  increase at the surface is also detected at higher altitudes, with about the same magnitude at Ivittuut between 7 July and 10 July and comparable magnitude at NEEM ( $+100$ ‰ for the marine grid point closest to NEEM) on 11 July. For this event, the water vapor monitored at the surface is thus representative of the water vapor at higher altitudes (here 3.5 to 6.5 km) and therefore of condensation water vapor. These remote sensing observations suffer from lower precision and are restricted to clear sky conditions, compared to in situ surface observations, which also give access to d-excess. The latter will thus be useful for an evaluation of water vapor isotopic composition and meteorology in this case study and can be used to evaluate the simulation of these parameters in AGCMs.

### 3.4. Simulation of Isotopic Distillation During Water Transport

The isotopic composition has been measured during the atmospheric river event at Ivittuut and NEEM, and we have identified a common moisture origin, transported toward both sites. To study the importance of Rayleigh distillation along transport, we compare the NEEM observations with the evolution of water vapor isotopic composition from Ivittuut to NEEM simulated with the MCIM model. These simulated and observed water vapor isotopic composition at Ivittuut and NEEM are presented in Figure 6.

For background summer conditions (June–July), as seen in Figure 6, due to the latitudinal temperature gradient between these two sites, MCIM produces a  $\delta D$  decrease explaining half of the observed gradient and a small increase in d-excess but not as large as observed. This is probably due to different summer moisture sources for the two sites (e.g., more Arctic moisture contributions for NEEM than Ivittuut), which is not taken into account in this calculation.

For the atmospheric river conditions, as seen in Figure 6, MCIM produces a reduced  $\delta D$  gradient (albeit not as small as observed) but fails to reproduce the observed d-excess level because it simulates a decrease

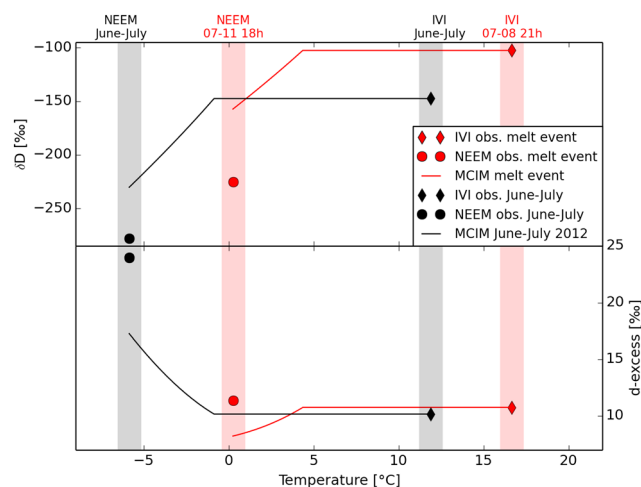


**Figure 6.** Idealized evolution of water vapor isotopic composition ( $\delta D$  and  $d$ -excess) between Ivittuut and NEEM against surface temperature, inferred from MCIM model simulation (plain curves) and from observations (diamonds for Ivittuut and circles for NEEM), for June–July 2012 period (black) and for the 10–11 July 2012 melt event (red). MCIM model water vapor isotopic composition is initialized with observed values at Ivittuut, and the model simulates its evolution when the temperature and atmospheric pressure goes from Ivittuut to NEEM observed values. The isotopic compositions and meteorological parameters correspond to the 2 month average conditions for the June–July period and to 8 July at 2100 h UTC at Ivittuut and 11 July at 1800 h UTC at NEEM for the melt event.

composition would help to refine the simulation setup by providing further constraints on the condensation vapor and temperature. Finally, processes related to droplet reevaporation associated with precipitation are not taken into account (which should contribute to the depletion of surface moisture as the reevaporated water originates from higher altitudes).

### 3.5. Simulations of Water Vapor Isotopic Composition

We now investigate the representation of the event in the most comprehensive AGCMs incorporating the explicit representation of water isotopes. Sensitivity tests are finally performed with different cloud parametrizations, in order to explore the impact of liquid cloud contents on meteorological parameters and water vapor isotopic composition in Greenland.

Figure 7 compares time series of daily averaged isotopic composition observed at Ivittuut and NEEM, with outputs from LMDz-iso and ECHAM5-wiso simulations, as well as MAR regional model outputs for near-surface  $T$  and  $q$ . The MAR outputs are taken at its first vertical level (2–3 m), while the LMDz-iso and ECHAM5-wiso outputs correspond to higher altitudes (respective levels top altitudes at about 20 and 8 hPa above ground level, thus around 160 and 70 m). First, consistent with earlier studies described in section 2.4, both LMDz-iso and ECHAM5-wiso models have a cold and dry bias at Ivittuut (with similar differences over July month of 5°C and 3 g/kg) and a wet and warm bias at NEEM (2°C and 1 g/kg). While they bracket the Ivittuut  $\delta D$  level, both models simulate too enriched  $\delta D$  levels at NEEM. LMDz-iso produces a reasonable level of  $d$ -excess at Ivittuut, even with too small variability, and strongly underestimates the mean level at NEEM. ECHAM5-wiso produces too low  $d$ -excess values at both sites, but the variability is more important than in LMDz-iso and closer to the observations. As expected for a regional model, MAR is the closest to observations for both  $T$  and  $q$ , with lower biases and a correct amplitude of variations. Model performance is systematically better at NEEM than at Ivittuut, where the spatial resolution of the models is not high enough to resolve the complex coastal topography around Ivittuut.

During the melt event, ECHAM5-wiso does not simulate the observed temperature increase at Ivittuut, while LMDz-iso underestimates this temperature variation and produces a maximum 1 day earlier than in observations (+5°C in LMDz-iso and +10°C in observations). At NEEM, both models produce temperatures

of  $d$ -excess level during transport. This discrepancy may indicate the contribution of additional moisture sources between NEEM and Ivittuut (e.g., droplet reevaporation and/or surface evaporation). However, as already pointed out, the MCIM simulation framework is not fully realistic and should not be expected to reproduce the real condensation conditions.

This simulation nevertheless highlights the importance of Rayleigh distillation occurring under positive temperatures during the whole melt event, leading to a similar  $d$ -excess level in South and northwest Greenland, in contrast with the usual latitudinal gradient. This calculation relies on the underlying assumptions that the condensation occurs at the same temperature as at the surface or that the water vapor isotopic composition is vertically homogeneous. This simplification partly explains the too enriched water vapor at NEEM in the model, as the condensation occurs at higher altitude than the surface.

Measurements of precipitation isotopic

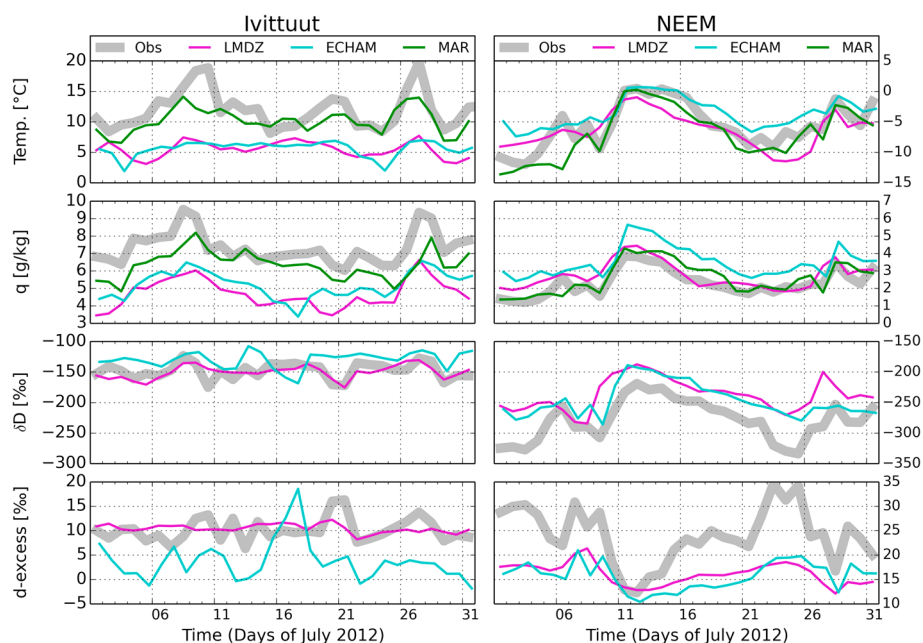


**Figure 7.** Observed (gray) and modeled LMDz-iso (magenta), ECHAM5-wiso (cyan), and MAR (green) daily averaged values for Ivittuut (left) and NEEM (right) of (downward): temperature ( $^{\circ}\text{C}$ ), specific humidity ( $\text{g}/\text{kg}$ ),  $\delta D$  ( $\text{‰}$ ), and d-excess ( $\text{‰}$ ).

close to  $0^{\circ}\text{C}$  during the warm event. Because they have a warm bias prior to and after this event, this again implies that they underestimate the magnitude of the event. Concerning the isotopic composition of surface water vapor, LMDz-iso and ECHAM5-wiso show only small changes in  $\delta D$  or d-excess at Ivittuut, which is consistent with the damped signal in daily averaged observations. They both capture the sharp increase in  $\delta D$  observed at NEEM, again with a faster increase for ECHAM5-wiso than LMDz-iso, consistent with model differences for  $q$  and  $T$ .

Sensitivity tests have been performed with LMDz-iso using different parametrizations of mixed clouds (see supporting information Text S2). As they affect the amount of liquid water and ice in clouds, they could potentially have an impact on water vapor isotopic composition. While the simulated  $T$  and  $q$  variations during the event at NEEM appear sensitive to these tests, no distinguishable impact on NEEM surface water vapor isotopic composition could be detected. The low-level cloud fraction observed and modeled at Ivittuut and NEEM is relatively small (10 to 20%) during the melt event (see supporting information Text S2). This might explain the small impact of mixed cloud parametrization of surface water vapor isotopic composition, within the very simplified representation of microphysical processes in LMDz-iso. This result suggests either that the water isotopes cannot be used to constrain the microphysical processes occurring in the mixed clouds or that the model representation of cloud composition is not adapted to this type of evaluation using surface water vapor isotopic composition. Further sensitivity tests on atmospheric models using different microphysics representations could thus be useful to distinguish the model gaps from the real processes.

Along the whole moisture path (Figure 5), we can only compare LMDz-iso outputs with IASI data, because we need to account for the specific vertical sensitivity of IASI retrievals (see section 2.2) and this implementation is not yet available for ECHAM5-wiso. The comparison shows that LMDz-iso correctly captures the timing of changes in midtropospheric  $q$  and  $\delta D$  at Ivittuut and NEEM. However, the mean values of both  $q$  and  $\delta D$  show large differences, only allowing for an investigation of variations rather than absolute values because of the lack of validation of IASI observations in this area.

Detailed investigation of the water vapor content and isotopic composition at the two stations from surface and upper level simulations and remote sensing observations as well as surface in situ observations (see Figure 8) shows that the magnitude of  $q$  and  $\delta D$  variations are in good agreement between LMDz-iso and IASI but again with significant moist biases (about  $1\text{ g}/\text{kg}$ ) in LMDz-iso for both stations and a  $\delta D$

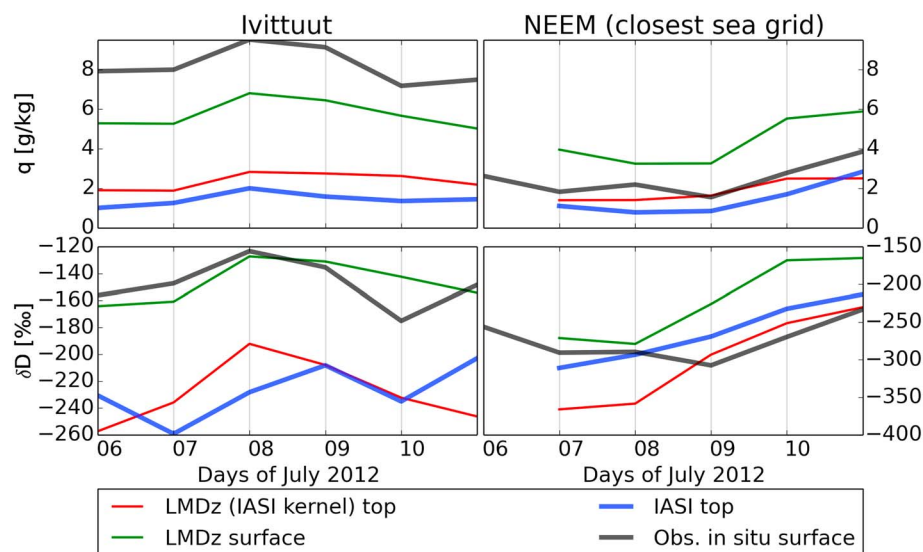


**Figure 8.** Specific humidity (top) and water vapor  $\delta D$  (bottom) evolution over Ivittuut (left) and NEEM closest oceanic grid cell (right), from 6 to 10 July 2012, extracted from IASI and surface observations (blue and black thick lines), LMDz-iso with IASI averaging kernel data at 3.5 and 6.5 km, and LMDz-iso data at the surface (green and red thin lines).

underestimation in Ivittuut (about 50‰). IASI outputs are only considered above the sea, which complicates the comparison with NEEM surface measurements. However, because of the elevation at NEEM, we observe small differences in absolute values of  $q$  and  $\delta D$  between NEEM surface data and IASI outputs at the closest sea grid point. At Ivittuut, the gap in absolute values is larger between surface and midtropospheric data. The evolution of  $q$  and  $\delta D$  at the end of the event (fast decrease between 9 and 10 July and new increase of 11 July) seems in better agreement between IASI and surface observations than between both observations data sets and LMDz-iso modeled values. LMDz-iso produces variations which are generally smoother than in observations. The timing of the  $\delta D$  maximum is delayed for 1 day in IASI compared to surface observations and LMDz-iso and does not correspond to the  $q$  maximum. As seen from the differences in  $\delta D$  evolution around Ivittuut between grid cells 18 and 19 in Figure 5, this is a very local pattern. It might be related with the alternating periods without and with cloud cover and precipitation around Ivittuut, which might affect the vertical profiles of water vapor isotopic composition (due to condensation or droplet reevaporation). The magnitude of  $q$  variations is approximately twice larger at the surface than in the midtroposphere, whereas similar  $\delta D$  amplitudes are recorded. Table 1 gives correlations between surface and midtropospheric  $q$  and  $\delta D$  estimated from LMDz-iso model and IASI and surface in situ observations. The comparison of LMDz-iso values at the two stations between surface and the upper altitude from 3.5 to 6.5 km shows that both surface and midtropospheric  $q$  and  $\delta D$  strongly covariate ( $R > 0.85$ ) in the model. In LMDz-iso, surface water vapor is therefore isotopically representative of midtropospheric water vapor (at the vertical location of IASI maximum of sensitivity). This is also the case when comparing the IASI and surface observations for  $q$  in Ivittuut and NEEM, as well as for  $\delta D$  at NEEM.

At Ivittuut, the delay between  $q$  and  $\delta D$  maxima depicted in IASI is not observed in surface data and not depicted by LMDz-iso. As a result, there is here no significant correlation between IASI and surface  $\delta D$  at Ivittuut. This may arise from the low signal-to-noise ratio in IASI data or from the small number of data points (short period of comparison), but it cannot be ruled out that upper altitude processes linked with cloudiness are not well reproduced by LMDz-iso. This can be due to physical parametrization or to the low model resolution (the grid might be too large to treat these small-scale cloud patterns).

### 3.6. Meteorological Conditions and Water Vapor Isotopic Composition in the Moisture Source Region

We now investigate the relation between water vapor isotopic composition in Greenland with that of the source region, at the time of moisture uptake, identified using our moisture source diagnostic.

Using the moisture source area identified by moisture source diagnostic based on backward trajectories, we extract the water vapor isotopic composition and meteorological data at the source.  $T$ , RH, and d-excess values from 1 to 9 July 2012 are reported in Table 2, extracted from three data sets: from LMDz-iso outputs

**Table 1.** Statistics of Linear Correlation Analysis<sup>a</sup> at Ivittuut and NEEM Calculated From Daily Averaged  $q$  and  $\delta D$  Values Between 6 July and 10 July 2012

		Ivittuut			NEEM		
		$R$	$N$	$p$ Value	$R$	$N$	$p$ Value
LMDz-iso surface LMDz-iso top	$q$	0.86	6	0.016	0.94	5	0.006
	$\delta D$	0.93	6	0.002	0.98	5	1e−4
IASI top LMDz-iso surface	$q$	0.82	6	0.031	0.92	5	0.009
	$\delta D$	0.36	6	0.466	0.97	5	0.001
LMDz-iso top observations surface	$q$	0.54	6	0.249	0.83	5	0.047
	$\delta D$	0.69	6	0.102	0.69	5	0.157
LMDz-iso surface observations surface	$q$	0.86	6	0.014	0.88	5	0.022
	$\delta D$	0.51	6	0.286	0.71	5	0.141
IASI top observations surface	$q$	0.72	6	0.085	0.95	5	0.004
	$\delta D$	0.24	6	0.645	0.78	5	0.084

<sup>a</sup>Correlation coefficients,  $R$ ; number of data points,  $N$ ;  $p$  value.

<sup>b</sup>Between LMDz-iso surface values and LMDz-iso values in the middle troposphere (3.5 to 6.5 km), between LMDz-iso surface values and IASI values in the middle troposphere (3.5 to 6.5 km), between LMDz-iso in the middle troposphere and surface in situ observations, and between IASI in the middle troposphere and surface in situ observations.

averaged over a band between 38.0 to 35.5°N and 71.25 to 48.75°W, from LMDz-iso outputs at one grid cell over the Bermuda Islands (31.69°N, 63.75°W), and from local observations at the same location [Steen-Larsen et al., 2014a].

During the moisture uptake period, high  $T$  and RH are observed over the subtropical Atlantic. This high humidity results from intense evaporation occurring after the advection of hot air masses coming from the American continent, also highlighted by Neff et al. [2014]. LMDz-iso indeed simulates  $T$  and RH of, respectively, 29°C and 90% on 1 July for the grid cell at 36.75°N and 78.75°W.

Concerning  $\delta D$ , the values simulated by LMDz-iso over the moisture source region vary between −81‰ and −74‰ during the event, which is close to the mean summer 2012 background values (−80‰ from June to August). This is slightly lower than that observed in Bermuda [Steen-Larsen et al., 2014a]. The data and model outputs depict 30‰ enriched  $\delta D$  values compared to those observed in South Greenland, clearly indicating distillation along northward transport.

**Table 2.** Averaged, Minimum, and Maximum Values of Relative Humidity (%),  $\delta D$  (‰) and d-excess (‰) Values From 1 to 9 July 2012, From Three Data Sets<sup>a</sup>

		LMDz-iso source region	LMDz-iso Bermuda Island	Observations Bermuda Island
Relative humidity (%)	Mean 1–9 July 2012	94.0	89.5	86.9
	Min 1–9 July 2012	92.2	82.9	80.2
	Max 1–9 July 2012	95.9	90.6	90.4
	Mean June–July	90.2	84.9	80.0
$\delta D$ (‰)	Mean 1–9 July 2012	−77.1	−85.3	−70.0
	Min 1–9 July 2012	−81.4	−92.6	−76.0
	Max 1–9 July 2012	−74.1	−78.0	−67.9
	Mean June–July	−81.3	−85.1	−77.0
d-excess (‰)	Mean 1–9 July 2012	5.8	11.6	4.1
	Min 1–9 July 2012	5.1	9.9	0.5
	Max 1–9 July 2012	6.9	12.7	8.4
	Mean June–July	7.4	11.6	7.8

<sup>a</sup>LMDz-iso outputs on a band of 38.0 to 35.5°N in latitude and 71.25 to 48.75°W in longitude, LMDz-iso outputs over the Bermuda Islands (31.69°N, 63.75°W), and observations from Bermuda station (32.26°N, 64.88°W).

Over Bermuda Islands, LMDz-iso depicts a wet bias compared to observations. As already well documented by the literature [Benetti *et al.*, 2014; Steen-Larsen *et al.*, 2014a; Pfahl and Sodemann, 2014], high RH at the source of evaporation causes low d-excess. From LMDz-iso in the moisture source region, the modeled d-excess of water vapor is lower during the moisture uptake period (5.8‰) than on average during summer 2012 (7.4‰ on June and July 2012). At the Bermuda Islands during the moisture uptake period, the model shows a higher d-excess (11.6‰) than the observations (4.1‰ on average). In general, during summer 2012 at Bermuda, LMDz-iso model underestimates the variability of d-excess and does not represent the lowest nor the highest observed d-excess values (not shown). As depicted by the moisture source diagnostic simulation, the moisture uptake has an important spatial variability, with very localized high evaporation spots over the subtropical Atlantic. Such spatial variability cannot be resolved by LMDz-iso at its low resolution. This may explain that the observed isotopic signal at Bermuda is closer to the LMDz-iso signal averaged over the complete moisture source region than to the LMDz-iso signal at the Bermuda grid cell.

The availability of water vapor isotopic measurements in Bermuda, close to the atmospheric river event moisture source, shows (i) distillation along transport, based on  $\delta D$  measurements, also consistent with IASI retrievals along the trajectory, and (ii) particularly low d-excess values (4–6‰), associated with moist and warm surface conditions, close to the level recorded in South and northwest Greenland. These findings provide the first observed case where d-excess is conserved during atmospheric transport.

#### 4. Conclusions and Perspectives

In this paper, we aimed to document the water vapor isotopic fingerprint of an atmospheric river leading to pervasive melt conditions in Greenland around 12 July 2012. We evaluate the potential of using observations of water vapor isotopic composition to determine the origins of humidity during this event, to study the physical processes affecting moisture during transport, to evaluate the cloud microphysics, and to assess the ability of AGCMs to simulate this type of events.

The remote sensing and in situ observations of water vapor isotopic composition presented here reveal that the variations recorded at the surface are closely related to those occurring in the free troposphere, despite some variations in remote sensing  $\delta D$  values which can either be attributed to observational noise or may result from changes in local cloudiness. Ivittuut coastal site in South Greenland depicts short-lived meteorological and  $\delta D$  variations and unusual parallel changes in d-excess. Sharp meteorological,  $\delta D$ , and d-excess changes occur a few days later in NEEM, and those anomalies persist during several days. NEEM d-excess reaches the same value as in Ivittuut, and half of  $\delta D$  difference between Ivittuut and NEEM can be explained by simple Rayleigh distillation occurring under positive temperatures, depicting common moisture sources. The d-excess signal in Greenland is also compatible with the isotopic composition of the water evaporated in the subtropical Atlantic from 30 to 40°N, following the eastward advection of an air mass from the American continent during an intense drought. The influence of this zone as an important moisture source was highlighted by atmospheric simulations: Lagrangian moisture source diagnostic showing an important evaporation along backward trajectories arriving to NEEM during the event; CHRM water tagging simulations confirming that this water vapor is conserved during transport and represent a dominant part of surface water vapor at both Ivittuut and NEEM (respectively, 40 and 30% of moisture originating from 30 to 50°N latitudinal band).

The evaluation of the representation of this particular event in atmospheric general circulation models (AGCMs) equipped with water isotopes has shown that those models do capture the evolution of  $T$ ,  $q$ , and water vapor isotopic composition for this event, reflecting the influence of large-scale processes. However, difficulties to simulate high d-excess prior to and after the event above the Greenland ice sheet indicate an incorrect representation of water vapor second-order isotopic composition, probably associated with Arctic moisture. This mismatch was already observed over Greenland [Steen-Larsen *et al.*, 2013; Bonne *et al.*, 2014] and might be related to misrepresentation of processes (e.g., kinetic effects at evaporation near sea ice margins) or the transport of the moisture originating from this region. New measurements of water vapor isotopic composition closer to the Arctic sources of evaporation (Svalbard, northern Siberia, on board *Polarstern*) should provide new information on processes at play. Preliminary sensitivity tests were performed here with LMDz-iso in order to assess the impact of cloud liquid water on water vapor isotopic composition, as this was suggested by Bennartz *et al.* [2013] to play a role in central Greenland surface climate. However, no significant conclusion arises from these tests. Thus, further investigation is needed

to understand the added value of Arctic moisture isotopic composition with respect to the representation of mixed cloud microphysics in atmospheric models and the importance of cloud feedbacks at NEEM. The regional model MAR was demonstrated to best reproduce the surface meteorological variations during the event. It would therefore be most interesting to integrate water vapor isotopes in this type of regional model, opening further possibilities to investigate cloud radiative properties and the impacts of cloud parametrizations on Greenland surface climate and water isotopic composition during this event.

This heat wave event has contributed to the understanding of mechanisms controlling d-excess variations above the Greenland ice sheet. The data support the fact that a strong signal in d-excess is related to moisture origin [Jouzel *et al.*, 2013]. We have demonstrated that d-excess in Greenland surface moisture decreases when moisture sources are predominantly of subtropical origin. This contradicts the interpretation of changes in ice core d-excess in terms of exclusive changes in sea surface temperature at the moisture source [Masson-Delmotte *et al.*, 2005] and supports the argument of the strong sensitivity of d-excess to surface RH [Jouzel *et al.*, 1982; Pfahl and Sodemann, 2014; Steen-Larsen *et al.*, 2014a]. This should motivate new investigation and interpretation of d-excess variations in ice cores and the climatic interpretation of melt layers recorded in ice cores.

Measurements of snow pit impurities were conducted at NEEM before and after the melt event. Before the melt event, the deposited impurities were within the normal range found for interglacial (Holocene) climate. Significantly elevated levels of  $\text{Na}^+$  were recorded following the melt event, which is consistent with deposition of moisture from an air mass with a high content of marine salts. Such an air mass likely took up marine moisture by strong convective updraft and experienced limited distillation between source and sink. This scenario is consistent with the d-excess measurements and moisture transport calculations. These isotopic and chemical fingerprints provide an indicator of similar circumstances driving past melt events found in ice core records.

Finally, this study shows the importance of a coordinated monitoring network combining (i) in situ data which provide high-resolution and high-accuracy information including d-excess and (ii) remote sensing products which allow to investigate changes in atmospheric composition at the moisture source and along the air mass trajectory. Our findings stress the added value of such measurements in order to constrain the origin of Arctic moisture, evaluate atmospheric models, and motivate the construction of a coordinated Arctic monitoring network.

In this manuscript, we have only investigated measurements performed in South and northwest Greenland. Another laser instrument has been operated in central Greenland on top of the ice sheet at Summit station during the 2012 summer season (D. Noone, personal communication, 2014). This opens the perspective to assess if the same atmospheric river fingerprint can be detected at Summit and to quantify surface snow-water vapor interactions [Steen-Larsen *et al.*, 2014b] occurring above the ice sheet under such exceptionally warm conditions.

This water vapor isotopic composition approach of atmospheric rivers analyses could also be applied to other locations such as east Antarctica, where atmospheric rivers strongly influence the ice sheet surface mass balance [Gorodetskaya *et al.*, 2014].

## Notation

d-excess	Deuterium excess
$T$	Specific humidity
RH	Relative humidity
$q$	Specific humidity
SST	Sea surface temperature

## References

- Alley, R. B., and S. Anandakrishnan (1995), Variations in melt-layer frequency in the GISP2 ice core: Implications for Holocene summer temperatures in central Greenland, *Ann. Glaciol.*, *21*, 64–70.
- Benetti, M., G. Reverdin, C. Pierre, L. Merlivat, C. Risi, H. C. Steen-Larsen, and F. Vimeux (2014), Deuterium excess in marine water vapor: Dependency on relative humidity and surface wind speed during evaporation, *J. Geophys. Res. Atmos.*, *119*, 584–593, doi:10.1002/2013JD020535.

## Acknowledgments

To access the data used in this publication, please refer to Jean-Louis Bonne (jean-louis.bonne@lsce.ipsl.fr). Ivittuut station is funded by IPEV, ICOS, CARBOOCEAN project, and ANR CEPS Green Greenland project (grant ANR-10-CEPL-0008) and operated by LSCE, France. We greatly thank the people involved in the observations at Ivittuut: Grnland Kommando GLK, Sermersooq Kummuneqarfik. NEEM is directed and organized by the Centre for Ice and Climate at the Niels Bohr Institute and US NSF, Office of Polar Programs. It is supported by funding agencies and institutions in Belgium (FNRS-CFB and FWO), Canada (GSC), China (CAS), Denmark (FIST), France (IPEV, INSU/CNRS and ANR VMC NEEM), Germany (AWI), Iceland (Rannís), Japan (NIPR), Korea (KOPRI), the Netherlands (NWO/ALW), Sweden (VR), Switzerland (SNF), the UK (NERC), and the USA (US NSF, Office of Polar Programs). Bermuda observatory is supported by the Danish Council for Independent Research (Natural Sciences grant 10-092850); the Carlsberg Foundation; the Icelandic Centre for Research (Equipment Fund grant 1202340031); CIRES Visiting Fellowship program; and the AXA Research Fund. LMDZ simulations were performed on the NEC supercomputer of the IDRIS computing center. IASI is a joint mission of EUMETSAT and the Centre National d'Études Spatiales (CNES, France). We thank the ULB/LATMOS teams for the IASI data processing.

- Bennartz, R., M. D. Shupe, D. D. Turner, V. P. Walden, K. Steffen, C. J. Cox, M. S. Kulie, N. B. Miller, and C. Pettersen (2013), July 2012 Greenland melt extent enhanced by low-level liquid clouds, *Nature*, 496(7443), 83–86, doi:10.1038/nature12002.
- Bonne, J.-L., V. Masson-Delmotte, O. Cattani, M. Delmotte, C. Risi, H. Sodemann, and H. C. Steen-Larsen (2014), The isotopic composition of water vapour and precipitation in Ivittuut, southern Greenland, *Atmos. Chem. Phys.*, 14(9), 4419–4439, doi:10.5194/acp-14-4419-2014.
- Cesana, G., and H. Chepfer (2012), How well do climate models simulate cloud vertical structure? A comparison between CALIPSO-GOCCP satellite observations and CMIP5 models, *Geophys. Res. Lett.*, 39, L20803, doi:10.1029/2012GL053153.
- Cesana, G., J. E. Kay, H. Chepfer, J. M. English, and G. de Boer (2012), Ubiquitous low-level liquid-containing Arctic clouds: New observations and climate model constraints from CALIPSO-GOCCP, *Geophys. Res. Lett.*, 39, L20804, doi:10.1029/2012GL053385.
- Ciais, P., and J. Jouzel (1994), Deuterium and oxygen 18 in precipitation: Isotopic model, including mixed cloud processes, *J. Geophys. Res. Atmos.*, 99(D8), 16,793–16,803, doi:10.1029/94JD00412.
- Coplen, T. B., P. J. Neiman, A. B. White, J. M. Landwehr, F. M. Ralph, and M. D. Dettinger (2008), Extreme changes in stable hydrogen isotopes and precipitation characteristics in a landfalling Pacific storm, *Geophys. Res. Lett.*, 35, L21808, doi:10.1029/2008GL035481.
- Craig, H., and L. I. Gordon (1965), *Deuterium and Oxygen 18 Variations in the Ocean and the Marine Atmosphere*, Consiglio nazionale delle ricerche, Laboratorio de geologia nucleare, Pisa, Italy.
- Dansgaard, W. (1964), Stable isotopes in precipitation, *Tellus*, 16(4), 436–468, doi:10.1111/j.2153-3490.1964.tb00181.x.
- de Boer, G., E. W. Eloranta, and M. D. Shupe (2009), Arctic mixed-phase stratiform cloud properties from multiple years of surface-based measurements at two high-latitude locations, *J. Atmos. Sci.*, 66(9), 2874–2887, doi:10.1175/2009JAS3029.1.
- De Ridder, K., and H. Gallée (1998), Land surface-induced regional climate change in southern Israel, *J. Appl. Meteorol.*, 37(11), 1470–1485, doi:10.1175/1520-0450(1998)037<1470:LSIRCC>2.0.CO;2.
- Dee, D. P., et al. (2011), The ERA-Interim reanalysis: Configuration and performance of the data assimilation system, *Q. J. R. Meteorol. Soc.*, 137(656), 553–597, doi:10.1002/qj.828.
- Fettweis, X., M. Tedesco, M. van den Broeke, and J. Ettema (2011), Melting trends over the Greenland ice sheet (1958–2009) from spaceborne microwave data and regional climate models, *Cryosphere*, 5(2), 359–375, doi:10.5194/tc-5-359-2011.
- Fettweis, X., E. Hanna, C. Lang, A. Belleflamme, M. Erpicum, and H. Gallée (2013), Brief communication: “Important role of the mid-tropospheric atmospheric circulation in the recent surface melt increase over the Greenland ice sheet”, *Cryosphere*, 7(1), 241–248, doi:10.5194/tc-7-241-2013.
- Gallée, H., and G. Schayes (1994), Development of a three-dimensional meso-gamma primitive equation model: Katabatic winds simulation in the area of Terra Nova Bay, Antarctica, *Mon. Weather Rev.*, 122(4), 671–685, doi:10.1175/1520-0493(1994)122<0671:DOATDM>2.0.CO;2.
- Gorodetskaya, I. V., M. Tsukernik, K. Claes, M. F. Ralph, W. D. Neff, and N. P. M. Van Lipzig (2014), The role of atmospheric rivers in anomalous snow accumulation in East Antarctica, *Geophys. Res. Lett.*, 41, 6199–6206, doi:10.1002/2014GL060881.
- Hourdin, F., et al. (2006), The LMDZ4 general circulation model: Climate performance and sensitivity to parametrized physics with emphasis on tropical convection, *Clim. Dyn.*, 27(7–8), 787–813, doi:10.1007/s00382-006-0158-0.
- Jouzel, J., L. Merlivat, and C. Lorius (1982), Deuterium excess in an East Antarctic ice core suggests higher relative humidity at the oceanic surface during the last glacial maximum, *Nature*, 299(5885), 688–691, doi:10.1038/299688a0.
- Jouzel, J., G. Delaygue, A. Landais, V. Masson-Delmotte, C. Risi, and F. Vimeux (2013), Water isotopes as tools to document oceanic sources of precipitation, *Water Resour. Res.*, 49(11), 7469–7486, doi:10.1002/2013WR013508.
- Klein, S. A., et al. (2009), Intercomparison of model simulations of mixed-phase clouds observed during the ARM Mixed-Phase Arctic Cloud Experiment. I: Single-layer cloud, *Q. J. R. Meteorol. Soc.*, 135(641), 979–1002, doi:10.1002/qj.416.
- Kurita, N. (2011), Origin of Arctic water vapor during the ice-growth season, *Geophys. Res. Lett.*, 38, L02709, doi:10.1029/2010GL046064.
- Lacour, J.-L., C. Risi, L. Clarisse, S. Bony, D. Hurtmans, C. Clerbaux, and P.-F. Coheur (2012), Mid-tropospheric deltaD observations from IASI/MetOp at high spatial and temporal resolution, *Atmos. Chem. Phys.*, 12(22), 10,817–10,832, doi:10.5194/acp-12-10817-2012.
- Masson-Delmotte, V., et al. (2005), Holocene climatic changes in Greenland: Different deuterium excess signals at Greenland Ice Core Project (GRIP) and NorthGRIP, *J. Geophys. Res.*, 110, D14102, doi:10.1029/2004JD005575.
- Meese, D. A., A. J. Gow, P. Grootes, M. Stuiver, P. A. Mayewski, G. A. Zielinski, M. Ram, K. C. Taylor, and E. D. Waddington (1994), The accumulation record from the GISP2 core as an indicator of climate change throughout the Holocene, *Science*, 266(5191), 1680–1682, doi:10.1126/science.266.5191.1680.
- Merlivat, L., and J. Jouzel (1979), Global climatic interpretation of the deuterium-oxygen 18 relationship for precipitation, *J. Geophys. Res.*, 84(C8), 5029–5033, doi:10.1029/JC084iC08p05029.
- NEEM-Community-Members (2013), Eemian interglacial reconstructed from a Greenland folded ice core, *Nature*, 493(7433), 489–494, doi:10.1038/nature11789.
- Neff, W., G. Compo, F. M. Ralph, and M. D. Shupe (2014), Continental heat anomalies and the extreme melting of the Greenland ice surface in 2012 and 1889, *J. Geophys. Res. Atmos.*, 119, 6520–6536, doi:10.1002/2014JD021470.
- Newell, R. E., N. E. Newell, Y. Zhu, and C. Scott (1992), Tropospheric rivers?—A pilot study, *Geophys. Res. Lett.*, 19(24), 2401–2404, doi:10.1029/92GL02916.
- Nghiem, S. V., D. K. Hall, T. L. Mote, M. Tedesco, M. R. Albert, K. Keegan, C. A. Shuman, N. E. DiGirolamo, and G. Neumann (2012), The extreme melt across the Greenland ice sheet in 2012, *Geophys. Res. Lett.*, 39, L20502, doi:10.1029/2012GL053611.
- Pfahl, S., and H. Sodemann (2014), What controls deuterium excess in global precipitation?, *Clim. Past*, 10(2), 771–781, doi:10.5194/cp-10-771-2014.
- Pommier, M., J.-L. Lacour, C. Risi, F. M. Bréon, C. Clerbaux, P.-F. Coheur, K. Gribanov, D. Hurtmans, J. Jouzel, and V. Zakharov (2014), Observation of tropospheric deltaD by IASI over western Siberia: Comparison with a general circulation model, *Atmos. Meas. Tech.*, 7(6), 1581–1595, doi:10.5194/amt-7-1581-2014.
- Rabier, F., H. Järvinen, E. Klinker, J.-F. Mahfouf, and A. Simmons (2000), The ECMWF operational implementation of four-dimensional variational assimilation. I: Experimental results with simplified physics, *Q. J. R. Meteorol. Soc.*, 126(564), 1143–1170, doi:10.1002/qj.49712656415.
- Ralph, F. M., and M. D. Dettinger (2011), Historical and national perspectives on extreme west coast precipitation associated with atmospheric rivers during December 2010, *Bull. Am. Meteorol. Soc.*, 93(6), 783–790, doi:10.1175/BAMS-D-11-00188.1.
- Rast, S., et al. (2013), User manual for ECHAM6, *Reports on Earth System Science 13*, Max Planck Institute for Meteorology, Hamburg, Germany.
- Risi, C., S. Bony, F. Vimeux, and J. Jouzel (2010), Water-stable isotopes in the LMDZ4 general circulation model: Model evaluation for present-day and past climates and applications to climatic interpretations of tropical isotopic records, *J. Geophys. Res.*, 115, D12118, doi:10.1029/2009JD013255.

- Roeckner, E., R. Brokopf, M. Esch, M. Giorgetta, S. Hagemann, L. Kornbluh, E. Manzini, U. Schlese, and U. Schulzweida (2006), Sensitivity of simulated climate to horizontal and vertical resolution in the ECHAM5 atmosphere model, *J. Clim.*, *19*(16), 3771–3791, doi:10.1175/JCLI3824.1.
- Schneider, M., et al. (2012), Ground-based remote sensing of tropospheric water vapour isotopologues within the project MUSICA, *Atmos. Meas. Tech.*, *5*(12), 3007–3027, doi:10.5194/amt-5-3007-2012.
- Shupe, M. D., S. Y. Matrosov, and T. Uttal (2006), Arctic mixed-phase cloud properties derived from surface-based sensors at SHEBA, *J. Atmos. Sci.*, *63*(2), 697–711, doi:10.1175/JAS3659.1.
- Sjolte, J., G. Hoffmann, S. J. Johnsen, B. M. Vinther, V. Masson-Delmotte, and C. Sturm (2011), Modeling the water isotopes in Greenland precipitation 1959–2001 with the meso-scale model REMO-iso, *J. Geophys. Res.*, *116*, D18105, doi:10.1029/2010JD015287.
- Sodemann, H., and A. Stohl (2013), Moisture origin and meridional transport in atmospheric rivers and their association with multiple cyclones, *Mon. Weather Rev.*, *141*(8), 2850–2868, doi:10.1175/MWR-D-12-00256.1.
- Sodemann, H., C. Schwierz, and H. Wernli (2008), Interannual variability of Greenland winter precipitation sources: Lagrangian moisture diagnostic and North Atlantic Oscillation influence, *J. Geophys. Res.*, *113*, D03107, doi:10.1029/2007JD008503.
- Sodemann, H., H. Wernli, and C. Schwierz (2009), Sources of water vapour contributing to the Elbe flood in August 2002—A tagging study in a mesoscale model, *Q. J. R. Meteorol. Soc.*, *135*(638), 205–223, doi:10.1002/qj.374.
- Steen-Larsen, H. C., et al. (2011), Understanding the climatic signal in the water stable isotope records from the NEEM shallow firn/ice cores in northwest Greenland, *J. Geophys. Res.*, *116*, D06108, doi:10.1029/2010JD014311.
- Steen-Larsen, H. C., et al. (2013), Continuous monitoring of summer surface water vapor isotopic composition above the Greenland Ice Sheet, *Atmos. Chem. Phys.*, *13*(9), 4815–4828, doi:10.5194/acp-13-4815-2013.
- Steen-Larsen, H. C., A. E. Sveinbjörnsdóttir, A. J. Peters, V. Masson-Delmotte, M. P. Guishard, G. Hsiao, J. Jouzel, D. Noone, J. K. Warren, and J. W. C. White (2014a), Climatic controls on water vapor deuterium excess in the marine boundary layer of the North Atlantic based on 500 days of in situ, continuous measurements, *Atmos. Chem. Phys.*, *14*(15), 7741–7756, doi:10.5194/acp-14-7741-2014.
- Steen-Larsen, H. C., et al. (2014b), What controls the isotopic composition of Greenland surface snow?, *Clim. Past*, *10*(1), 377–392, doi:10.5194/cp-10-377-2014.
- Stohl, A., C. Forster, A. Frank, P. Seibert, and G. Wotawa (2005), Technical note: The Lagrangian particle dispersion model FLEXPART version 6.2, *Atmos. Chem. Phys.*, *5*(9), 2461–2474, doi:10.5194/acp-5-2461-2005.
- Stohl, A., C. Forster, and H. Sodemann (2008), Remote sources of water vapor forming precipitation on the Norwegian west coast at 60°N—A tale of hurricanes and an atmospheric river, *J. Geophys. Res.*, *113*, D05102, doi:10.1029/2007JD009006.
- Tedesco, M., X. Fettweis, T. Mote, J. Wahr, P. Alexander, J. E. Box, and B. Wouters (2013), Evidence and analysis of 2012 Greenland records from spaceborne observations, a regional climate model and reanalysis data, *Cryosphere*, *7*(2), 615–630, doi:10.5194/tc-7-615-2013.
- Vidale, P. L., D. Lüthi, C. Frei, S. I. Seneviratne, and C. Schär (2003), Predictability and uncertainty in a regional climate model, *J. Geophys. Res.*, *108*(D18), 4586, doi:10.1029/2002JD002810.
- Werner, M., and M. Heimann (2002), Modeling interannual variability of water isotopes in Greenland and Antarctica, *J. Geophys. Res.*, *107*(D1), 4001, doi:10.1029/2001JD900253.
- Werner, M., P. M. Langebroek, T. Carlsen, M. Herold, and G. Lohmann (2011), Stable water isotopes in the ECHAM5 general circulation model: Toward high-resolution isotope modeling on a global scale, *J. Geophys. Res.*, *116*, D15109, doi:10.1029/2011JD015681.
- Yoshimura, K., M. Kanamitsu, and M. Dettinger (2010), Regional downscaling for stable water isotopes: A case study of an atmospheric river event, *J. Geophys. Res.*, *115*, D18114, doi:10.1029/2010JD014032.
- Zhu, Y., and R. E. Newell (1998), A proposed algorithm for moisture fluxes from atmospheric rivers, *Mon. Weather Rev.*, *126*(3), 725–735, doi:10.1175/1520-0493(1998)126<0725:APAFMF>2.0.CO;2.